

# The Distance and Metallicity of the Newly Discovered, Nearby Irregular Galaxy HIZSS3<sup>1</sup>

David R. Silva

*European Southern Observatory*

*Karl-Schwarzschild-Str. 2, Garching bei München, D-85748, Germany*

dsilva@eso.org

and

Philip Massey

*Lowell Observatory*

*1400 W. Mars Hill Road, Flagstaff, AZ, 86001, USA*

Phil.Massey@lowell.edu

and

Kathleen DeGioia-Eastwood

*Department of Physics and Astronomy*

*Northern Arizona University, P.O. Box 6010, Flagstaff, AZ, 86011-6010, USA*

Kathy.Eastwood@nau.edu

and

P. A. Henning

*Institute for Astrophysics*

*University of New Mexico, 800 Yale Boulevard, NE, Albuquerque, NM, 87131-1156, USA*

henning@as.unm.edu

## ABSTRACT

HIZSS3 is an H I source in the Zone of Avoidance. Its radio characteristics are consistent with it being a previously unknown nearby ( $\sim 1.8$  Mpc) low-mass dwarf irregular (dIm) galaxy. Optical observations have shown that it contains a modest H II region but failed to reveal a resolved stellar population. New spectroscopic observations of the H II region obtained at the MMT Observatory are presented here. They are used to derive the line-of-sight extinction ( $E(B - V) = 1.41 \pm 0.04$ ) and gas metallicity ( $\log O/H + 12 \sim 7.8$ ) of the H II region. New near-IR imaging observations obtained at the ESO Very Large Telescope are also presented here. These images clearly reveal the resolved stellar population of HIZSS3 for the first time. Narrow-band  $P\beta$  images of the H II region are used in combination with previously published  $H\alpha$  data to obtain an independent line-of-sight extinction estimate:  $E(B - V) = 1.32 \pm 0.04$ . The adopted foreground extinction is  $E(B - V) = 1.36 \pm 0.06$ . Based on the K-band luminosity function and  $K, J - K$  color-magnitude diagram, the apparent magnitude and color of the tip of the red-giant branch (TRGB) are derived. In turn, these parameters are combined with the adopted foreground extinction to estimate the distance ( $1.69 \pm 0.07$  Mpc) and mean red giant branch metallicity ( $[Fe/H] = -0.5 \pm 0.1$ ). As an ensemble, these new observations significantly strengthen the conclusion that HIZSS3 is a newly discovered low-mass dIm lurking behind the Milky Way in the outskirts of the Local Group.

## 1. Introduction

HIZSS3 ( $l = 217.7$ ,  $b = 0.01$ ) is an H I source in the Zone of Avoidance (ZOA), i.e. the region near the Galactic plane where foreground extinction from dust and gas causes an apparent decrease in the surface density of extragalactic objects at optical wavelengths. HIZSS3 was originally detected at 21-cm by the Dwingeloo Obscured Galaxies Survey (Henning et al. 1998; Rivers, Henning, & Kraan-Korteweg 1999; Rivers 2000) and the H I Parkes Zone of Avoidance Shallow Survey (Henning et al. 2000). The name (HIZSS3) comes from the list in the latter paper. Based on Very Large Array (VLA) observations, it has an H I mass of  $2 \times 10^7 M_{\odot}$ , assuming a distance of 1.8 Mpc estimated from the heliocentric velocity ( $280 \text{ km s}^{-1}$ ) of the H I source transformed to the Local Group velocity centroid and assuming no peculiar velocity (Massey, Henning, & Kraan-Korteweg 2003, hereafter MHK2003). Given the low radial velocity of the H I gas, this distance (and hence mass) estimate must be considered unreliable. A modest H $\alpha$  source at the same heliocentric velocity and within the VLA 21-cm contours of HIZSS3 was detected by MHK2003. This star-formation site is not spatially coincident with the main, resolved H I peak in the MHK2003 VLA 21-cm map, but rather with a semi-resolved secondary peak. *BVRI* images obtained by MHK2003 centered on the 21-cm peak failed to detect definitively any stars associated with HIZSS3, likely due to a combination of poor seeing ( $\sim 3$  arcsec) and high foreground extinction (estimated  $A_B = 4.7$  mags; Henning et al. 2000).

As discussed by MHK2003, the characteristics of HIZSS3 suggest that it is a newly discovered, nearby dwarf irregular galaxy (dIm). At an estimated distance of 1.8 Mpc, HIZSS3 lies beyond the zero-velocity boundary of the Local Group. However, this 21-cm redshift based distance estimate relies on the assumption that HIZSS3 has negligible peculiar velocity which is true for most, but not all (e.g. Leo I), Local Group members. Thus, Local Group membership cannot be ruled out based

on existing radio data.

In this paper, new data are presented from the European Southern Observatory Very Large Telescope and MMT Observatory facilities. The MMTO spectroscopic observations are used to measure foreground reddening and the nebular metallicity of the H II region detected by MHK2003. Foreground reddening is independently estimated using VLT near-IR photometric observations and a different methodology. The two foreground reddening estimates are found to be essentially identical. More significantly, the stellar component of HIZSS3 is directly observed for the first time in near-IR images obtained with the VLT. Using these images, near-IR luminosity functions as well as a color-magnitude diagram (CMD) are constructed. In combination, these functions and the CMD are used to estimate the metallicity and distance of the tip of the red-giant branch (TRGB). In agreement with MHK2003, the new derived properties of HIZSS3 presented here are consistent with a previously unknown dwarf irregular galaxy on the outskirts of the Local Group.

## 2. Observations & Data Processing

### 2.1. MMTO Observations

Optical spectroscopy of the H II region found in HIZSS3 by MHK2003 was obtained on 2003 November 21 UT at the 6.5m MMT Observatory by PM and KDE. The primary goal of these observations was to determine foreground reddening from spectrophotometry of H $\beta$  relative to H $\alpha$ , with a secondary goal of determining the oxygen abundance if the [O II]  $\lambda 3727$  nebular line could be detected despite the high reddening. The data were obtained with the MMT Blue Channel spectrograph using a  $500 \text{ l mm}^{-1}$  grating with a dispersion of  $1.18 \text{ \AA pixel}^{-1}$  using a  $2688 \times 512$  backside-processed CCD provided by the University of Arizona Imaging Technology Lab. In order to allow in more light, the slit was opened to 3.5 arcsec, resulting in a resolution of 10 pixels ( $12 \text{ \AA}$ ). No blocking filter was used in order to maximize the throughput, a seemingly safe choice given that first-order H $\alpha$  would be contaminated by second-order light at  $3280 \text{ \AA}$ . While this proved to be a good choice for the H II region, the bluest flux standards (G191B2B and Feige 34) showed evi-

---

<sup>1</sup>The optical spectroscopic observations reported here were obtained at the MMT Observatory, a joint facility of the Smithsonian Institution and the University of Arizona. The near-IR imaging observations reported here were collected at the European Southern Observatory, Cerro Paranal, Chile, within observing program 271.B-5047.

dence of a 10% contamination in the red compared to the flux standard Hiltner 600, which has a large Balmer jump. Thus, only observations of the latter were used for the flux calibration. The HIZSS3 observations were made as eight 1200 sec integrations, with the slit of the spectrograph reset to the parallactic angle at the beginning of each integration.

IRAF<sup>1</sup> was used for all data processing. Examination of the two-dimensional spectra revealed that the spatial distribution of the nebular lines was localized to 1 – 2 arcsec, coincident with the H II region. The spectra were extracted using the trace of an observation of the nearby offset star as the template. Sky background was determined from each side of the extraction aperture and subtracted. There is obvious structure within the slit due to brightness variations of the nebula, and this structure changed with the rotation angle. Therefore, the intensities of the strongest lines (H $\alpha$ , H $\beta$ , and [OIII]  $\lambda$  5007) were measured from each individual spectrum. The spectra went deep enough to detect [OII]  $\lambda$ 3727, although this line and the N[II]  $\lambda$ 6584 lines were so weak that they could only be measured in the co-added spectrum. Three pertinent regions are shown in Fig. 1

The relative emission-line strengths are given in Table 1. The actual H $\alpha$  flux measured is only about one-quarter the total H $\alpha$  luminosity measured from direct images by MHK2003. This is due presumably to slit losses necessitated by remaining at the parallactic angle (position angle  $\sim$  0 degrees) that prevented the slit from being aligned with the H II region (position angle  $\sim$  130 degrees; see Fig. 3 of MHK2003).

## 2.2. VLT Observations

### 2.2.1. HIZSS3 and Reference Field

Near-IR imaging observations of HIZSS3 and a nearby reference field were obtained at the ESO Very Large Telescope during 2003 November. Time for these images was allocated within the ESO Director’s Discretionary Time (DDT) program. All VLT observations reported here

<sup>1</sup>The Image Reduction and Analysis Facility (IRAF) is distributed by the National Optical Astronomy Observatories, which are operated by the Association of Universities for Research in Astronomy, Inc., under contract with the National Science Foundation.

were executed in Service Mode.

Images were obtained using the short-wavelength (SW) arm of the ISAAC near-IR imaging spectrometer mounted at one of the Nasymth foci of the Antu/UT1 8.2m telescope. The SW arm uses a 1024x1024 Hawaii Rockwell HgCdTe array with a plate scale of 0.148 arcsec pix<sup>-1</sup> for a single-image field-of-view of approximately 2.5  $\times$  2.5 arcmin. ISAAC was operated in its standard jitter mode, where a series of images is obtained with random telescope offsets of up to 15 arcsecs relative to a fiducial center point between each individual exposure.

A series of such jittered images was obtained for both the HIZSS3 field ( $\alpha = 07^{\text{h}}00^{\text{m}}26^{\text{s}}.9$ ,  $\delta = -04^{\circ}12'30''$ , J2000) and a nearby reference field ( $\alpha = 07^{\text{h}}00^{\text{m}}11^{\text{s}}.0$ ,  $\delta = -04^{\circ}03'38''$ , J2000) in the  $J_s$  and  $K_s$  filters. The HIZSS3 field center was chosen to include both the 21-cm peak and the H II region discussed in MHK2003 (see that work for coordinates). The reference field was selected to have the identical galactic latitude and contain no very bright stars. It is otherwise unexceptional and located approximately 10 arcmins away. An additional narrow-band  $P\beta$  image (ISAAC filter NB\_1.28) of the HIZSS3 field was obtained to allow the determination of foreground reddening. All images were obtained under clear, apparently photometric, conditions (see photometric calibration discussion below). A summary of these observations is provided in Table 2.

The HIZSS3 and reference field image series were processed by the ESO ISAAC pipeline into single images which were dark, bias, and background corrected. These images were delivered as part of the standard ESO Service Mode data package. Images were processed using the *combine\_mc* algorithm, reported to produce photometrically reliable final images<sup>2</sup>. Photometric accuracy was verified by comparing the instrumental magnitudes of stars detected in single frames with the same stars in the combined frames. No systematic trends with respect to position or magnitude were seen within the area where all images in the series overlapped, confirming the photometric reliability of the pipeline output.

Five output images were delivered:  $J_s$  and  $K_s$  images for both the HIZSS3 and reference field

<sup>2</sup>See <http://www.eso.org/projects/aot/eclipse/jitterphot/>.

pointings, as well as  $P\beta$  for the HIZSS3 pointing. All five output images were trimmed to the same area, corresponding to the output image with the smallest area where all input images for that stack overlapped. The final size of the trimmed images was 951 x 951 pixels, corresponding to 19,810 arcsec<sup>2</sup> or 5.503 arcmin<sup>2</sup>. The image quality of the output images is excellent: the FWHM of a Gaussian fit to the FWHM is close to 0.5 arcsecs in the  $J_s$  and  $K_s$  frames and 0.6 arcsecs in the  $P\beta$  frame.

These images clearly reveal the stellar content of HIZSS3 for the first time. The  $K_s$  HIZSS3 and reference field images are shown in Figure 2. The reference field image simply shows a uniform distribution of stars, while the HIZSS3 field image clearly shows enhanced object surface density at the locations of the H II region and the H I peak. Figure 3 shows zoomed  $J_s$ ,  $K_s$ , and  $P\beta$  images of the H II region. This latter figure clearly shows stellar objects associated with the nebular gas.

### 2.2.2. Photometric Calibration

The ESO calibration program provides nightly observations of UKIRT photometric standards (Hawarden et al. 2001) for ISAAC SW imaging observations. Additional observations of red UKIRT standards were obtained in  $J_s$  and  $P\beta$  on the same nights that the HIZSS3  $P\beta$  observations were obtained. A summary of the relevant standard stars observations is found in Table 2.

Input images of  $J$  and  $K$  UKIRT standards for all three nights were processed by the ESO pipeline into standard images that were dark, bias, and background corrected. These output images were delivered as part of the standard ESO Service Mode data package. The  $P\beta$  standard images were not processed by the ESO pipeline because the NB\_1.28 filter is not supported by the standard pipeline. Therefore, input images were processed manually to correct for bias, dark, and (minimal) background.

The instrumental magnitudes of the  $J$  and  $K$  UKIRT standards were measured using standard IRAF aperture photometry tools. Apertures of radii 15 pixels (2.22 arcsecs) were used, with sky annulus radii 20 pixels (2.96 arcsecs) and widths 10 pixels (1.48 arcsecs). Each star was observed as a sequence of five observations at different physical locations on the array – essentially, center, upper

left, upper right, lower right, and lower left. For each star, the mean and standard deviation was computed from the five individual observations. In all cases, the standard deviation was approximately 0.03 mag. This uncertainty is typical for observations for photometric standards with infrared arrays. It does not arise from photon counting related statistical reasons but from a combination of uncertainties from flat-fielding and illumination corrections, light losses from inter-pixel gaps, bad pixels, and intra-pixel sensitivity variations.

Photometric transformation zeropoints ( $\zeta_i$ ) were computed from each standard star observation using the following equation:

$$\zeta_i = m_i^{cat} - m_i^{ins} - \kappa_i X$$

where  $i$  is the filter,  $X$  is the airmass,  $m_i^{cat}$  is the catalog magnitude,  $m_i^{ins}$  is the mean instrumental magnitude (i.e. the mean of the five individual measurements), and  $\kappa_i$  is the adopted extinction coefficient. For  $J_s$  and  $K_s$ , telluric extinction coefficients of  $-0.07$  and  $-0.05$ , respectively, were chosen to minimise the scatter between individual zeropoint measurements. These values are consistent with the mean values stated in the *ISAAC User's Manual*. Not enough standard stars were observed to determine reliable color terms independently. However, the ISAAC color terms are thought to be negligible (C. Lidman, private communication).

Final nightly zeropoints were computed by computing the mean (and standard deviation) of the individual observations. For 2003 November 7 and 9 UT, the  $J_s$  zeropoints are  $24.71 \pm 0.025$  (5 stars) and  $24.77 \pm 0.004$  (2 stars). For 2003 November 8 and 9 UT, the  $K_s$  zeropoints are  $24.16 \pm 0.003$  (2 stars) and  $24.14 \pm 0.003$  (2 stars). Combined with the adopted extinction coefficients, these zeropoints transform instrumental magnitudes into  $J$  and  $K$  in the UKIRT system (Hawarden et al. 2001; see that work for transformations to other systems).

The formal uncertainties of the nightly zeropoints do not provide a definitive constraint on the photometric quality of the relevant nights because of the relatively small number of standard stars observed (see Table 2). What can be said is: (1) these measured zeropoint values are con-

sistent with the values reported on the ISAAC quality control Web site<sup>3</sup> over a long time period, once aperture differences are taken into account; (2) measurements separated by hours on the same night produce zeropoints consistent to within a few percent; and (3) variations in atmospheric transmission measured by the Paranal Ambient Site Monitor (ASM) were less than 0.02 mag in the R-band during the entire night for all three nights<sup>4</sup>. In conclusion, the nights during which these VLT observations occurred appear to be have been photometric at the 0.02 mag or better level.

### 3. Analysis

#### 3.1. Foreground Extinction

Relative emission-line strengths measured in the H II region are given in Table 1. Using the Cardelli, Clayton, & Mathis (1989) reddening law ( $A_{H\beta} = 3.609E(B - V)$  and  $A_{H\alpha} = 2.535E(B - V)$ ) and an intrinsic ratio  $H\beta/H\alpha=0.350$ , the derived foreground reddening is  $E(B - V) = 1.41 \pm 0.04$ , where the error represents the standard deviation of the mean for the 8 individual ratios. Using this extinction, corrected flux ratios are given in Table 1. The reddening-corrected line ratio  $[OIII] \lambda 5007$  to  $[OIII] \lambda 4959$  is 2.8, in good agreement with the 2.9 value expected on theoretical grounds.

The VLT  $P\beta$  images of the H II region can be used to make a similar but independent measurement of the foreground reddening, namely by comparing the flux of the H II region at  $P\beta$  ( $1.28\mu\text{m}$ ) to that at  $H\alpha$ . This technique has been recently exploited in a study of spiral galaxies by Jones, Elston, & Hunter (2002). The only complication is the lack of spectrophotometric standards in the near-IR, necessitating the use of model atmospheres with JHK standards. We are indebted to L. Jones for correspondence and advice on this subject.

The UKIRT standards (Hawarden et al. 2001) FS 112 (G0) and FS 121 (K3) were observed through the ISAAC narrow band  $1.28\mu\text{m}$  filter (NB\_1.28) as well as the broadband  $J_s$  and  $K_s$

<sup>3</sup>See <http://www.eso.org/qc/>.

<sup>4</sup>See <http://archive.eso.org/asm/ambient-server>. As Start-Night, use the UT Date minus one (1) day. For Site, select Paranal.

filters. The Kurucz (1992) Atlas 9  $\log g = 4.5$ ,  $T_{\text{eff}} = 6000^\circ\text{K}$  and  $4750^\circ\text{K}$  models were adopted for these two stars. For each model, the average fluxes within the  $J_s$  and  $K_s$  filters were computed. For each star, a conversion factor between model flux (in physical units) and observed flux (in ADUs per second) was computed using the Hawarden et al. catalog magnitudes, under the assumption that  $J_s = 0$  and  $K_s = 0$  for Vega. The conversion factors for the two stars agreed within 10%, providing confidence in this procedure.

These conversion factors were then used to transform observed NB\_1.28 flux into absolute flux. In order to determine an emission-line flux for a line-source, the width of the filter must also be taken into account, i.e.  $\int T_\lambda d\lambda / T_{1.28\mu\text{m}} = 194$ , where  $T_\lambda$  is the transmission of the filter as a function of wavelength<sup>5</sup>. The  $P\beta$  count rate was then measured after aligning the  $J_s$  image to  $P\beta$ , and subtracting after matching the PSFs by convolution and scaling. The derived flux at  $P\beta$  is  $9.88 \times 10^{-15}$  ergs  $\text{cm}^{-2}$   $\text{s}^{-1}$ . The observed ratio  $(P\beta/H\alpha = 8.7 \times 10^{-2})_{\text{obs}} = 0.45$  (where the flux at  $H\alpha$  has been taken from MHK2003) can be compared to the intrinsic ratio  $(P\beta/H\alpha = 8.7 \times 10^{-2})_{\text{int}} = 5.71 \times 10^{-2}$  (Osterbrock 1974). Combined with the Cardelli et al. (1989) reddening law, the foreground reddening was found to be  $E(B - V) = 1.32 \pm 0.04$ . This is in good agreement with the value found from the MMT0 optical spectroscopy ( $1.41 \pm 0.04$ ).

The computed mean and standard deviation of these two foreground reddening measurements is  $E(B - V) = 1.36 \pm 0.06$ . If 1.25 microns and 2.2 microns are adopted as the effective wavelengths of the  $J_s$  and  $K_s$  bands, respectively, the Cardelli et al. reddening curve can be used to compute  $A(J - K)$ :  $A_{1.25} = A_J = 0.874 \times E(B - V) = 1.19 \pm 0.06$  mag and  $A_{2.2} = A_K = 0.352 \times E(B - V) = 0.48 \pm 0.06$  mag. Therefore,  $A_J - A_K = E(J - K) = 0.522 \times E(B - V) = 0.71 \pm 0.06$  mag.

Formally, these foreground extinction measurements are only valid for the line-of-sight to the H II region. It is quite possible the foreground extinction across the HIZSS3 field is variable, either due to variations in the foreground Galac-

<sup>5</sup>See Jacoby, Africano, and Quigley (1987), but beware of an error in equation 3, in which  $F_N(i)$  is used in place of the correct quantity  $F(i)$

tic dust distribution or due to (hypothetical) dust within HIZSS3 itself. For example, the H II region could be more dusty than the rest of HIZSS3. It is impossible to constrain the magnitude of possible spatially variable foreground reddening without detailed spectrophotometry of the individual stars in HIZSS3. Thus, a single-valued  $E(B - V)$  is adopted for the rest of this paper. As discussed later, this does not have a significant impact on the main conclusions of this work.

### 3.2. HII Region Metallicity

Without detection of the temperature-sensitive [OIII] $\lambda$ 4363 line, quasi-empirical relations between other emission line ratios and oxygen abundance (the so-called  $R_{23}$  method) may be used to approximate the metallicity of the H II region (Pagel et al. 1979). Three approaches are possible<sup>6</sup>:

(1) **Classical  $R_{23}$  method.** The  $R_{23}$  ratio

$$R_{23} = \frac{[\text{OIII}]\lambda 5007 + [\text{OIII}]\lambda 4959 + [\text{OII}]\lambda 3727}{\text{H}\beta} = 5.50$$

has been calibrated by Skillman (1989) for the case that the oxygen abundance is much lower than solar. Using his formula results in a value  $\log O/H + 12 = 7.5$ .

(2)  **$R_{23}$  method modified by [OIII]/[NII].** Edmunds & Pagel (1984) use a modified version of the  $R_{23}$  method, which relies upon using the strength of the N[II] $\lambda$ 6584 line as an additional calibration of  $R_{23}$ . The current measurements result in

$$\log \frac{[\text{OIII}]\lambda 5007 + [\text{OIII}]\lambda 4959}{[\text{NII}]\lambda 6584} = 2.22,$$

yielding a value of  $\log O/H + 12 = 7.8$ .

(3)  **$R_{23}$  method modified by [OIII]/[OII].** McGaugh (1991) instead calibrates the  $R_{23}$  value with the relative strengths of [OIII] and [OII]:

$$\log \frac{[\text{OIII}]\lambda 5007 + [\text{OIII}]\lambda 4959}{[\text{OII}]\lambda 3727} = 0.35.$$

This yields a value of  $\log O/H + 12 = 7.85$ .

In summary,  $\log O/H + 12 \sim 7.8$ , comparable to other metal-poor irregular galaxies in the Local Group, i.e., IC 1613 ( $\log O/H+12=7.85$ ; Talent

1980), WLM ( $\log O/H+12=7.77$ ; Hodge & Miller 1985), and Pegasus ( $\log O/H+12=7.93$ ; Skillman, Bomans, & Kobulnicky 1997). For comparison, the oxygen abundances of the LMC and SMC are 8.37 and 8.13, respectively (Russell & Dopita 1990), while that of the solar neighborhood is 8.70 (Esteban & Peimbert 1995).

### 3.3. Photometric Properties of Resolved Stellar Population

Stellar objects were identified in the  $K_s$  HIZSS3 and reference field images using the DAOPHOT star finding routine implemented under IRAF. This routine identifies features that are significantly above the local noise (in this case,  $3\sigma$ ) and whose roundness and sharpness are typical of stars. After removing objects that fell partially on the edge of the images, 528 objects were detected in the reference field and 739 in the HIZSS3 field. Although a small percentage of these stellar objects are undoubtedly unresolved background objects at high redshift, we assume henceforth that all the detected objects are stars in the Milky Way or HIZSS3. As can be seen in Figure 2, the stellar surface density in the HIZSS3 field is higher near the positions of the H I peak and H II regions reported by MHK2003. In the reference field, the stellar surface density is more uniform.

Instrumental aperture magnitudes of the detected stars were measured using IRAF aperture photometry tools. Point spread function matching was deemed unnecessary given the relatively low stellar surface density (see Figure 2). Instrumental magnitudes were measured through a 5-pixel (0.74 arcsec) radius circular aperture, using background measurements local to each star. Using the same aperture properties and the pixel coordinates of the stars detected on the  $K_s$  frames, aperture magnitudes were also measured on the  $J_s$  frames after each  $J_s$  frame was geometrically aligned with the corresponding  $K_s$  frame to sub-pixel accuracy. A small number of objects in the  $K_s$  reference and HIZSS3 images (3 and 12, respectively) were so faint in the corresponding  $J_s$  images that  $J_s$  magnitudes could not be measured.

These instrumental magnitudes were transformed to the UKIRT system using the photometric zeropoints and extinction terms described in the last section. An aperture correction from

<sup>6</sup>We thank D. Hunter for her guidance in this matter.

the 5-pixel radius used for the program stars to the 15-pixel radius used for the standard stars was computed using a few isolated stars in the program fields. This transformation process was repeated independently for all four HIZSS3 and reference field frames.

The result is a stellar catalog with  $J$  and  $K$  magnitudes (and corresponding errors) in the UKIRT near-IR photometric system. Note that these magnitudes have *not* been corrected for foreground reddening. In principle, such a correction is possible for stars associated with HIZSS3 by ignoring possible variations in the foreground dust distribution. As shown below, however, stars can only be assigned to HIZSS3 on a statistical basis, making *a priori* extinction corrections of individual magnitudes impossible – a foreground extinction correction can only be made to ensemble properties. It is also impossible to correct foreground stars for extinction because it cannot be assumed they lie at a common distance and therefore a simple screen model cannot be assumed.

Using this catalog, the luminosity functions shown in Figure 4 were constructed. Bin widths are set to 0.4 mag to improve the statistical significance in each bin. In both panels, the dashed (blue) lines are the 525 stars with  $J$  and  $K$  magnitudes in the reference field and the solid (black) lines are the 727 stars with  $J$  and  $K$  magnitudes in the HIZSS3 field.

Since HIZSS3 contains only one modest H II region, star formation is clearly not happening throughout the bulk of the galaxy. Thus, the brightest stars in the near-IR should be stars at or near the tip of the first-ascent giant branch (TRGB). In principle, the apparent magnitude and color of the TRGB can be used to constrain distance and metallicity. To detect the TRGB, the methodology of Lee, Freedman, & Madore (1993) is adopted. For a range of histogram bin sizes, the HIZSS3 and reference field  $K$  luminosity functions are constructed and then subtracted to produce a background corrected  $K$  luminosity function for HIZSS3. Each background subtracted luminosity function is then convolved with a 3-element edge detector filter with the values  $[-2,0,+2]$  (i.e. the so-called zero-sum Sobel kernel). The resultant vector has local maxima at the luminosities where histogram discontinuities occur. The center of the *next* luminosity bin is then adopted as the TRGB

apparent magnitude. Figure 5 provides illustrative examples for bin sizes of 0.1 and 0.5 mag, corresponding to TRGB edges at  $K = 19.80$  and  $20.00$ , respectively.

TRGB edges were determined for bin sizes 0.10, 0.15, 0.20, 0.25, 0.30, 0.35, 0.40, 0.45, and 0.50 mag. For these nine bins, the mean and standard deviation of the TRGB edge brightness is  $K = 19.90 \pm 0.09$ . This value is consistent with a visual inspection of the luminosity functions shown in Figure 4. After correction for foreground extinction ( $A_{2.2} = 0.48 \pm 0.06$ , see Section 3.1), this value corresponds to  $K_0 = 19.42 \pm 0.11$ , where the edge brightness uncertainty and the foreground reddening uncertainty have been added in quadrature.

From deeper near-IR observations in the literature, it is known that object count should continue to increase with magnitude. This is clearly not the case here, as shown in Figure 4. Estimates of the apparent magnitude where sample incompleteness becomes significant can be made by applying the Sobel edge detection methodology again. For each field and each filter, total luminosity functions (i.e. without background subtraction) were constructed for bin sizes between 0.5 and 0.1 mag using steps of 0.05 mag. Each luminosity function was then convolved with the same 3-element edge detection filter as above. For most resultant vectors, significant incompleteness is indicated by the global minimum. The *previous* (i.e. next brighter) bin is adopted as the completeness limit. The mean and standard deviation over all bin sizes are then computed for each field and filter.

The  $K$  completeness limits for the HIZSS3 and reference images were found to be  $21.18 \pm 0.09$  and  $21.34 \pm 0.21$ , respectively - that is, the same within the errors. The corresponding  $J$  completeness limits are  $23.33 \pm 0.11$  and  $23.26 \pm 0.21$  - again, the same within the errors. In both filters, the uncertainty of the reference field completeness limit is larger due to the detection of fewer sources.

The object catalog constructed above can also be used to construct the HIZSS3 and reference field color-magnitude diagrams shown in Figure 6. Only objects with  $\sigma_{J-K} \leq 0.5$  are shown. In the HIZSS3 field, there are 44 objects with color uncertainties larger than 0.5 mag, including 12 objects with no measurable  $J$  magnitude. In the reference field, the corresponding numbers are 8 and 3.

Looking at Figure 6, it is clear that there are more stars with  $J - K \approx 1.9$  in the HIZSS3 field than in the reference field. This is further quantified in Figure 7 which shows that this excess lies in the approximate color range  $1.6 < J - K < 2.2$  for stars with  $K > 19.5$  (i.e. slightly above TRGB and fainter) and  $\sigma_{JK} \leq 0.2$  mag. For these criteria, there are significantly more objects (141) in the HIZSS3 field than in the reference field (39). These objects are adopted as red giant branch (RGB) candidates in HIZSS3. The spatial distribution of these RGB candidates is shown in Figure 8. The RGB candidates are preferentially clumped near the VLA 21-cm HI peak and the HII region, while bluer and redder stars are more uniformly distributed. The median color of the RGB candidates in the HIZSS3 field is  $J - K = 1.87 \pm 0.1$ , corresponding to  $(J - K)_0 = 1.16 \pm 0.12$  after extinction correction where the color uncertainty has been added in quadrature with the foreground extinction uncertainty. The 13 objects spatially coincident with the H II region emission-line gas are circled in Figure 6. About half (6) of these objects are bluer than the RGB candidates, consistent with them being hotter stars.

### 3.4. Stellar Metallicity and Distance Estimates

Using the extinction corrected apparent magnitude of the TRGB ( $K_0 = 19.42 \pm 0.11$ ) and adopted median TRGB color ( $(J - K)_0 = 1.16 \pm 0.12$ ), the metallicity and distance to HIZSS3 can be estimated by comparing the observed HIZSS3 properties to the properties of Galactic globular clusters as presented by Valenti, Ferraro, & Origlia (2004a,b). These papers are preferred over older papers by the same team (e.g. Ferraro et al. 2000) because all the Galactic globular cluster data have been transformed in a uniform way to the 2MASS photometric system.

Using the UKIRT-2MASS color transformations found on the 2MASS Web site<sup>7</sup>, the adopted median RGB color becomes  $J - K_0 = 1.23$  on the 2MASS system. A similar UKIRT-2MASS transformation of  $K_0$  is not necessary given the small (0.003) color term in the published transformation equation. The transformed median TRGB color is consistent with the TRGB colors of the most

metal-rich Galactic globular clusters (see Valenti et al. 2004a, Figure 3) where  $[Fe/H]$  lies in the range  $-0.5 \pm 0.1$ .

Recall that in the H II region,  $[O/H] \sim 7.8 - 8.7 = -0.9$ , i.e. the nebular gas appears to be significantly more metal-poor than the stars near the TRGB. One speculative explanation for this difference is that the star formation event traced by the H II region is being fueled by gas falling into HIZSS3 for the first time. In this regard, it should be noted that the H II region lies in a bulge of the H I gas (see MHK2003). It is possible that this bulge represents recently arrived gas. Higher spatial resolution velocity maps of the H I gas would be very helpful for investigating this possibility. Such images are currently being obtained and analyzed.

From Valenti et al. (2004b),  $M_{K_s, 2MASS}^{TRGB} \sim -6.7 \pm 0.1$  for metal-rich Galactic globular clusters. Using  $K_0 = 19.42 \pm 0.11$  as the foreground extinction-corrected TRGB apparent magnitude (see above), a HIZSS3 distance modulus of  $26.12 \pm 0.14$  or  $1.69 \pm 0.07$  Mpc is implied. Note that  $M_K^{TRGB}$  varies slowly with TRGB metallicity and thus color (see, e.g., Valenti et al. 2004b, Figure 5). The fact that the adopted TRGB color/metallicity is somewhat uncertain does not have a major impact on the adopted  $M_K^{TRGB}$ . Hence, it does not have a major impact on the distance modulus uncertainty. The TRGB-based distance estimate is remarkably consistent with the 21-cm redshift estimate of 1.8 Mpc published by MHK2003.

Values for the TRGB apparent magnitude and median RGB color have been set from the aggregate properties of stars distributed spatially across the entire HIZSS3 field. However, a measurement of  $E(B - V)$  is only available along one line-of-sight, i.e. to the H II region contained within HIZSS3. If this H II region is more dusty than the rest of HIZSS3, the foreground extinction correction for the TRGB apparent magnitude would be smaller, increasing the estimated distance to HIZSS3. However, the corrected median RGB color would also become redder, reaching values in excess of median RGB colors of Galactic globular clusters, which seems unlikely. Spatially variable foreground extinction is also possible, but its effects (if present) would be limited to increasing intrinsic  $E(B - V)$  uncertainty and thus distance

<sup>7</sup><http://www.astro.caltech.edu/jmc/2mass/v3/transformations/>



measurement uncertainty. In summary, the adoption of a single-valued  $E(B - V)$  does not have a significant impact on the measurement of mean stellar distance or metallicity.

#### 4. Conclusions

Using data obtained at the MMT Observatory and ESO Very Large Telescope, the following new properties of HIZSS3 have been derived:

1. A resolved stellar population has been revealed for the first time. Its near-IR properties are consistent with a TRGB apparent magnitude of  $K_0 = 19.42 \pm 0.11$  and a median TRGB color of  $(J - K)_0 = 1.22 \pm 0.12$ .
2. The line-of-sight extinction to the H II region was found to be  $E(B - V) = 1.41 \pm 0.04$  based on long-slit spectroscopic observations and  $E(B - V) = 1.32 \pm 0.04$  based on narrow-band  $H\alpha$  and  $P\beta$  observations. Given the various uncertainties, this agreement is excellent. The adopted foreground extinction is  $E(B - V) = 1.36 \pm 0.06$  for the near-IR photometric measurements.
3. Based on emission-line equivalent width measurements, the H II region metallicity was found to be  $\log O/H + 12 \sim 7.8$ , corresponding to  $[O/H] \sim -0.9$ . In contrast, the mean RGB metallicity was estimated to be  $[Fe/H] = -0.5 \pm 0.1$  based on TRGB color. In other words, stars on the RGB appear to be somewhat more metal-rich than the nebular gas. This difference could be explained if the star formation event traced by the H II emission has been fed by lower metallicity gas falling into HIZSS3 for the first time. Higher spatial resolution maps of the H I gas have been obtained and will be analyzed to investigate this possibility.
4. Using the derived TRGB apparent magnitude of  $K_0 = 19.42 \pm 0.11$  and an adopted absolute magnitude of  $-6.7 \pm 0.1$ , the HIZSS3 distance modulus was found to be  $26.12 \pm 0.14$ , corresponding to a physical distance of  $1.69 \pm 0.07$  Mpc. This estimate is in excellent agreement with distance estimate of  $\sim 1.8$  Mpc derived from 21-cm redshifts under

the assumption of zero peculiar velocity with respect to the Local Group velocity centroid.

These newly derived quantities significantly strengthen the conclusion that HIZSS3 is a newly discovered dIm lurking at the edge of the Local Group. As discussed by MHK2003, HIZSS3 appears to be the nearest dIm discovered in the last 25 years. However, the TRGB distance estimate presented here ( $\sim 1.7$  Mpc) supports the MHK2003 conclusion that HIZSS3 is *not* a member of the Local Group, having more in common with galaxies at a similar distance as Sextans A, Sextans B, NGC 3109, and Antlia.

We thank the ESO Director's Discretionary Time Committee (DDTC) for approving the ESO observations. We also thank Lowell Tacconi-Garman, Emmanuel Jehin, and Wolfgang Hummel for their end-to-end assistance with the VLT observations. We gratefully acknowledge several useful conversations with Deidre Hunter and Lauren Jones. PM acknowledges support from NSF grant AST0093060. Finally, we thank the anonymous referee for helpful comments and suggestions.

VLT(ISAAC) MMTO(Blue Channel Spectrograph)

#### REFERENCES

- Cardelli, J. A., Clayton, G. C., & Mathis, J. S. 1989, ApJ, 345, 245
- Edmunds, M.G., & Pagel, B.E.J., 1984, MNRAS, 211, 507
- Esteban, C., & Peimbert, M. 1995, Rev. Mex. Astron. Astrofis. Ser. Conf. 3, 133
- Ferraro, F.R., Montegriffo, P., Origlia, L., Fusi Pecci, F. 2000, AJ, 119, 1282
- Hawarden, T. G., Leggett, S. K., Letawsky, M. B., Ballantyne, D. R., & Casali, M. M. 2001, MNRAS, 325, 563
- Henning, P.A., Kraan-Korteweg, R.C., Rivers, A.J., Loan, A.J., Lahav, O., & Burton, W.B. 1998, AJ, 115, 584
- Henning, P.A. et al. 2000, AJ, 119, 2686
- Hodge, P. & Miller, B. W. 1995, ApJ, 451, 176
- Jacoby, G. H., Africano, J. L., & Quigley, R. J. 1987, PASP, 99, 672

- Jones, L. V., Elston, R. J. & Hunter, D. A. 2002, AJ, 124, 2548
- Kurucz, R. L. 1992, in The Stellar Populations of Galaxies, ed. B. Barbuy & A. Renzini (Dordrecht, Kluwer), 225
- Lee, M.G., Freedman, W.L., & Madore, B.F. 1993, ApJ, 417, 559
- Massey, P., Henning, P. A., & Kraan-Korteweg, R. C. 2003, AJ, 126, 236 (MHK2003)
- McGaugh, S. S. 1991, ApJ, 380, 140
- Osterbrock, D. 1974, Astrophysics of Gaseous Nebulae (Freeman: San Francisco)
- Pagel, B. E. J., Edmunds, M. G., Blackwell, D. E., Chun, M. S., & Smith, G. 1979, MNRAS, 189, 95
- Rivers, A.J., Henning, P.A., & Kraan-Korteweg, R.C., 1999, Publ. Astron. Soc. Australia, 16, 48
- Rivers, A.J. 2000, Ph. D. thesis, Univ. of New Mexico
- Russell, S. C., & Dopita, M. A. 1990, ApJS, 84, 93
- Skillman, E. D. 1989, ApJ, 347, 883
- Skillman, E. D., Bomans, D. J., Kobulnicky, H. A. 1997, ApJ, 474, 205
- Talent, D. L. 1980, PhD Thesis, Rice Univ.
- Valenti, E., Ferraro, F.R., & Origlia, L. 2004a, MNRAS, in press. (astro-ph/0403563)
- Valenti, E., Ferraro, F.R., & Origlia, L. 2004a, MNRAS, in press. (astro-ph/040403)

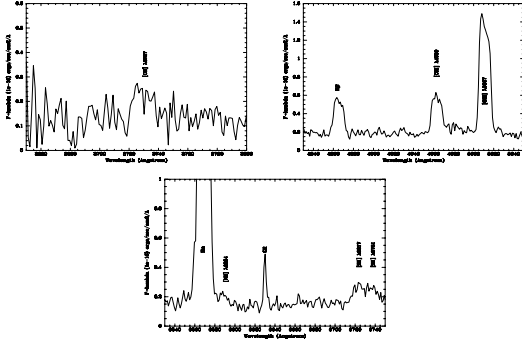


Fig. 1.— Three spectral regions in our summed spectrum of the H II region in HIZSS3 are shown.

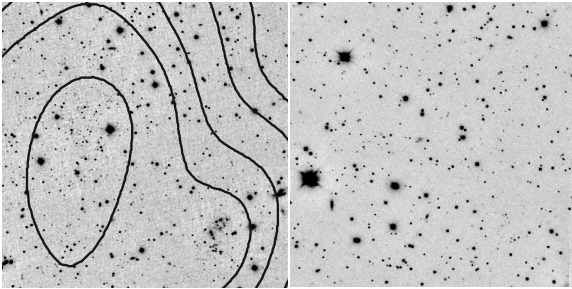


Fig. 2.—  $K_s$  HIZSS3 (left) and reference field (right) images. North is up, east is left. Each image is  $2.35 \times 2.35$  arcmin in size. In the HIZSS3 image, the H I contours from MHK2003 are overlaid (see their Figure 1). From inspection, it is clear that there is a faint stellar population associated with the H I peak while the H II region lies within a bulge in the H I contours. Objects in the reference field are more uniformly distributed and less numerous.

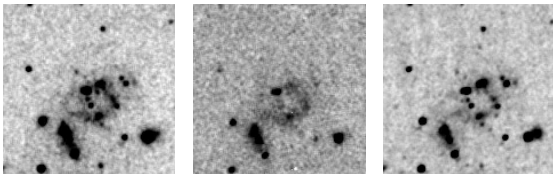


Fig. 3.— Cut-out images of the H II region detected by MHK2003. From left-to-right:  $J_s$ ,  $P\beta$ , and  $K_s$ . North is up, east is left. Each image is  $22 \times 22$  arcsecs.

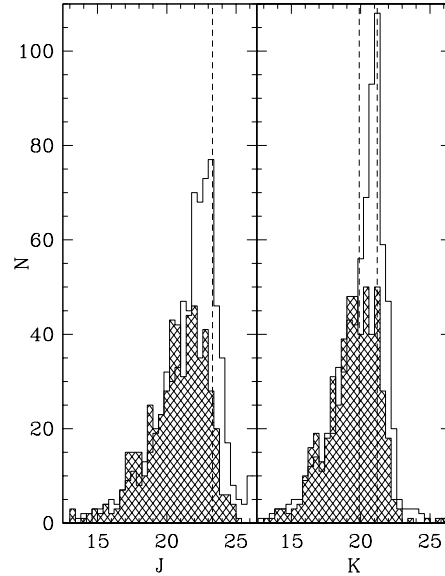


Fig. 4.—  $J$  and  $K$  luminosity functions for the stellar objects in the HIZSS3 and reference field images with  $J$  and  $K$  magnitudes. The bin size is 0.4 mag. The hashed luminosity functions contain the 525 stellar objects in the reference field. The non-hashed luminosity functions contain the 727 stellar objects in the HIZSS3 field. The vertical dashed line in the  $J$  panel indicates the completeness limit in the HIZSS3 field. The vertical dashed lines in the  $K$  panel indicate the adopted TRGB apparent magnitude and the completeness limit in the HIZSS3 field.

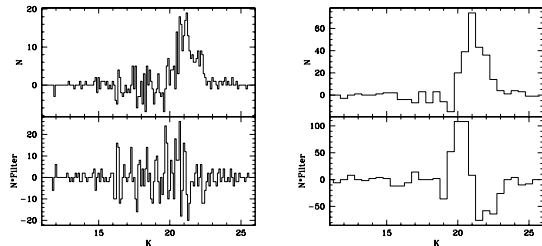


Fig. 5.— Background corrected K-band luminosity function for HIZSS3 field before (top panels) and after (lower panels) convolution with Sobel  $[-2, 0, +2]$  edge detection filter. Two bin sizes are shown: 0.1 mag (left) and 0.5 mag (right).

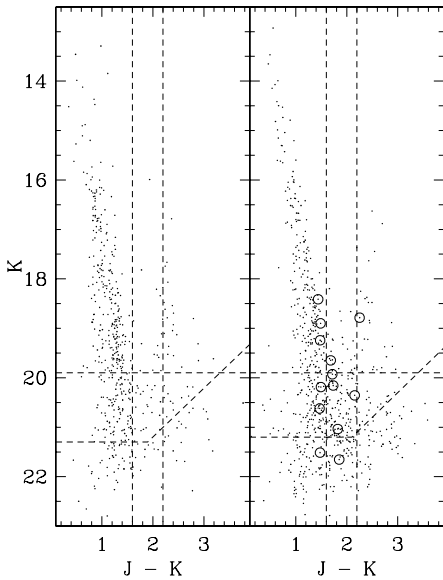


Fig. 6.— Color-magnitude diagrams for reference (left) and HIZSS3 (right) fields. Only stars with  $\sigma_{J-K} \leq 0.5$  mag are shown. The HIZSS3 TRGB edge at  $K = 19.90 \pm 0.09$  is indicated by a horizontal dashed line. The combination of the  $J$  and  $K$  completeness limits are shown as connected dashed horizontal and diagonal lines. The vertical dashed lines indicate the color region that contains the RGB candidates in the HIZSS3 field. The circled objects in the HIZSS3 (right) panel indicate stars that are spatially coincident with the H II region emission-line gas. See text for more details.

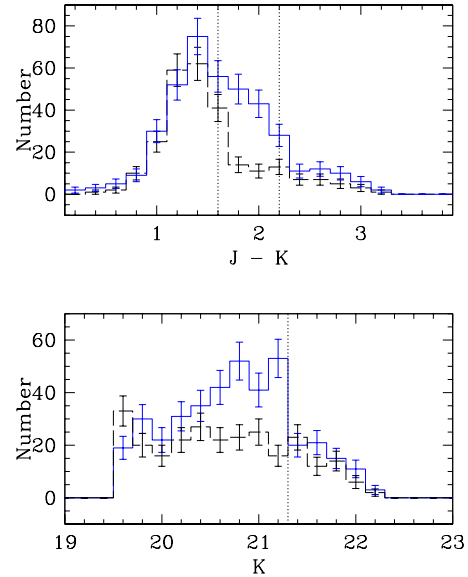


Fig. 7.— Color and luminosity distributions used to select RGB candidates. Only stars with  $K > 19.5$  and  $\sigma_{J-K} \leq 0.2$  are shown. Neither color nor luminosity are corrected for foreground extinction. In both panels, the solid (blue in on-line version) histogram shows the HIZSS3 stellar distribution while the dashed (black in on-line version) line shows the distribution of objects in the reference field. In the color distribution panel, the vertical dashed lines delineate the color range of the candidate RGB stars in HIZSS3 (see text). In the luminosity panel, the vertical dashed line shows the adopted  $K$  completeness limit.

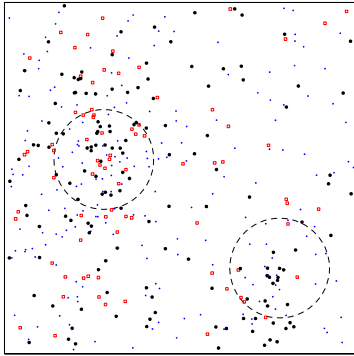


Fig. 8.— Distribution of objects in HIZSS3 field grouped by color. North is up, east is left, and the field-of-view is  $2.35 \times 2.35$  arcmins in size (compare to HIZSS3  $K_s$  image shown in Figure 2). Only objects with  $K \geq 19.9$  and  $\sigma_{J-K} \leq 0.5$  are shown. Small filled (blue in on-line version) circles correspond to  $J - K < 1.6$ . Large filled (black in on-line version) circles correspond to  $1.6 \leq J - K \leq 2.2$  (i.e. the HIZSS3 red giant candidates). Open (red in on-line version) squares correspond to  $J - K > 2.2$ . The upper dashed circle is centered on the VLA HI peak while the lower dashed circle is centered on the HII region. Circle centers correspond to coordinates published by MHK2003. The circle radii are 20 arcsecs.

TABLE 1  
RELATIVE EMISSION-LINE STRENGTHS

Spectral Line	Uncorrected Flux	Corrected Flux
[OII] $\lambda$ 3727	0.033	0.60
[OII] $\lambda$ 4959	0.10	0.35
[OIII] $\lambda$ 5007	0.29	0.98
H $\beta$	0.087	0.35
H $\alpha$	1.000	1.00
[NII] $\lambda$ 6584	0.0080	0.0080

TABLE 2  
VLT OBSERVATION LOG

UT Date+Time	Target	Integration (s)	Filter	Airmass	Seeing (arcsecs)
2003 Nov 06 23:40	UKIRT FS29	5 $\times$ 14.2	$J_s$	1.12	...
2003 Nov 07 00:12	UKIRT FS6	5 $\times$ 14.2	$J_s$	2.30	...
2003 Nov 07 04:55	UKIRT FS6	5 $\times$ 14.2	$J_s$	1.18	...
2003 Nov 07 07:00	UKIRT FS112	5 $\times$ 20.0	$P\beta$	1.09	...
2003 Nov 07 07:11	HIZSS3	11 $\times$ 180	$P\beta$	1.11	0.60
2003 Nov 07 07:54	UKIRT FS121	5 $\times$ 20.0	$P\beta$	1.09	...
2003 Nov 07 08:00	UKIRT FS121	5 $\times$ 20.0	$J_s$	1.10	...
2003 Nov 07 08:08	HIZSS3	30 $\times$ 60	$J_s$	1.11	0.53
2003 Nov 07 23:52	UKIRT FS29	5 $\times$ 14.2	$K_s$	1.30	...
2003 Nov 08 07:43	HIZSS3	35 $\times$ 60	$K_s$	1.07	0.49
2003 Nov 08 09:01	UKIRT FS14	5 $\times$ 14.2	$K_s$	1.10	...
2003 Nov 08 09:27	UKIRT FS10	5 $\times$ 14.2	$K_s$	2.28	...
2003 Nov 09 03:50	UKIRT FS6	5 $\times$ 14.2	$J_s$	1.15	...
2003 Nov 09 04:03	UKIRT FS6	5 $\times$ 14.2	$K_s$	1.15	...
2003 Nov 09 06:11	Off-Field	35 $\times$ 60	$K_s$	1.21	0.50
2003 Nov 09 07:10	Off-Field	30 $\times$ 60	$J_s$	1.10	0.48
2003 Nov 09 08:57	UKIRT FS14	5 $\times$ 14.2	$J_s$	1.10	...
2003 Nov 09 09:09	UKIRT FS14	5 $\times$ 14.2	$K_s$	1.10	...

NOTE.—UT Time+Date indicates start of observing sequence. Seeing is reported for final combined images produced by ISAAC pipeline. Seeing is not reported for standard stars.